UNIVERSITAT POLITÈCNICA
DE CATALUNYA

Report on theoretical results of power generation and conversion

Carles Batlle, Arnau Dòria Cerezo, Enric Fossas

ACES: Control Avançat de Sistemes d'Energia

IOC-DT-P-2006-14
Abril 2006

Institut d'Organització i Control
de Sistemes Industrials

Report on theoretical results of Power Generation and Conversion.

Carles Batlle, Arnau Dòria-Cerezo and Enric Fossas
Institut d'Organització i Control de Sistemes Industrials
Universitat Politècnica de Catalunya

April, 2006

Abstract

Theoretical results of the Flywheel Energy Storage System are presented. This report summarizes the main theoretical results obtained in the context of the GeoPlex European project, using a Hamiltonian-based description of the problem. The power policy management is also studied paying special attention to the optimal speed of the doubly-fed induction machine, and this constitutes the main contribution of this report. Finally, using the control laws designed in the IDA-PBC framework, simulation results are showed and commented.

Keyboards: Flywheel Energy Storage System, power flow management.
Paraules clau: Sistema d'emmagatzement d'energia cinètica, gestió de flux de potència.
Palabras clave: Sistema de almacenamiento de energía cinética, gestión del flujo de potencia.

Contents

1 Introduction

The system studied in this workpackage is an autonomous energy–switching system that regulates the energy flow between a local prime mover (a flywheel) and the electrical power network, in order to satisfy the demand of a time–varying electrical load. This system, used in the CERN (Centre Européen pour la Recherche Nucléaire) to store electrical energy for the particle accelerator or at the Okinawa Electric Power Company [1], has been also studied in [1]. The main goal of the system is, basically, to store kinetic energy into a flywheel and deliver it when an external load requires a high energy flow.

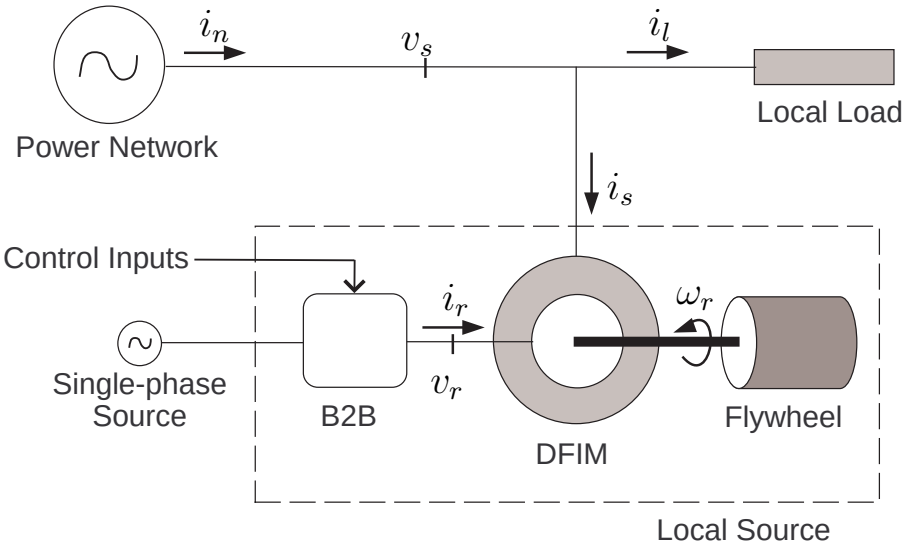

Figure 1: Doubly fed induction machine coupled to a flywheel, controlled by a back-to-back converter and connected to a power network and a load.

The system (see Figure 1) is composed by a doubly–fed induction machine (DFIM) coupled to a flywheel and controlled through the rotor windings by a back-to-back converter (B2B). This is the most common control architecture of the DFIM [1][7][9][10][11][12][13][15] , typically achieved by means of a B2B. In a case that the AC source of the B2B is connected to the 3-phase power grid, this architecture is also known as Scherbius Drive [9], *i.e.* the power converter is in a closed–loop with the DFIM. In practice, due to the fact that the power flowing through the power converter is smaller than the power flowing to the DFIM stator side, it is common to neglect this *feedback* connection.

The DFIM is controlled through the rotor windings port ($v_r, i_r \in \mathbb{R}^3$, where v and i are a three-phase voltage and current variables, and subindex r refers to the rotor). It is coupled to an energy–storing flywheel with port variables (τ_e electrical torque, ω mechanical speed). An electrical network modelled by an ideal AC voltage source with port variables ($v_n, i_n \in \mathbb{R}^3$ subindex n refers to the network variables), and a generic electrical three-phase load, represented by its impedance Z_l, is connected to the stator port variables ($v_s, i_s \in \mathbb{R}^3$).

As mentioned above, the main objective of the system is to supply the required power to the load with a high network power factor. Depending on the load demands, the DFIM acts as an energy–switching device between the flywheel and the electrical power network. The control problem is to optimally regulate the power flow.

These goals, assuming a maximal active power of the network P_n^{MAX}, can be summarized as follows:

- **To supply** the extra energy required by the load. Notice that this objective concerns the active power, and considering a constant grid voltage, $V_n = ct$, this requirement is achieved by the stator currents.
- **To store** kinetic energy in the flywheel when the load does not require all the grid power.
- **To compensate** the power factor ($\cos\phi$), i.e., the whole system (load and local source acts as a pure resistor). That is $\cos\phi \sim 0$, or, in other words assuming, sinusoidal waveform and an equilibrated system, this objective can be written as $Q_n \sim 0$.

This control problem can be achieved by commuting between different steady–state regimes. The switching strategy was studied in [5].

2 The Port-controlled Hamiltonian Model

In this Section we recall the port-Hamiltonian description of the whole system. The interconnection rules between the power converter and the doubly-fed induction machine (DFIM), basically the dq-transformation, are extensively studied in [2].

Port-controlled Hamiltonian Systems (PCHS) describe, from an energetic point of view, a large kind of systems [6]. An explicit PCHS has the form

$$\begin{cases} \dot{x} = (\mathcal{J}(x) - \mathcal{R}(x))(\nabla H(x))^T + g(x)u \\ y = g^T(x)(\nabla H(x))^T \end{cases} \tag{1}$$

where $x \in \mathbb{R}^n$ are the energy variables, $H(x) : \mathbb{R}^n \to \mathbb{R}$ is the energy (or Hamiltonian) function, $u, y \in \mathbb{R}^m$ are the port variables, $\mathcal{J}(x) = -\mathcal{J}^T(x) \in \mathbb{R}^{n\times n}$ is the intra-connection structure matrix, describing how the energy flows inside the system, $\mathcal{R} = \mathcal{R}^T \geq 0 \in \mathbb{R}^{n\times n}$ is the dissipation matrix, and $g(x) \in \mathbb{R}^{n\times m}$ is the interconnection matrix, describing the port connection of the system to the outside world. Port variables are conjugated, so that $[u][y]$ has units of power. Non-negativeness of $\mathcal{R}$ ensures that the map $u \to y$ is passive [14].

2.1 The Doubly-fed Induction Machine coupled to a flywheel

A Port-controlled Hamiltonian model of a DFIM coupled to a flywheel is given in [4]. This model is described in dq-coordinates [8], so that three-phase variables (abc) are reduced to two-phase variables (dq). The variables are (the D subindex refers to the DFIM subsystem) $x_D^T = (\lambda_s^T, \lambda_r^T, J_m\omega) \in \mathbb{R}^5$, or $x_D^T = (\Lambda^T, x_m)$, where $\Lambda^T = (\lambda_s^T, \lambda_r^T) \in \mathbb{R}^4$, $\lambda_s,\ \lambda_r \in \mathbb{R}^2$ are the inductor fluxes in dq-coordinates (stator and rotor respectively), $x_m = J_m\omega$ is the mechanical Hamiltonian variable, ω the angular speed of the rotor, and J_m is the total moment of inertia of the rotating parts. The structure $\mathcal{J}_D \in \mathbb{R}^{5\times 5}$ and

damping $\mathcal{R}_D \in \mathbb{R}^{5\times5}$ matrices are

$$\mathcal{J}_D = \begin{pmatrix} -\omega_s L_s J_2 & -\omega_s L_{sr} J_2 & O_{2\times1} \\ -\omega_s L_{sr} J_2 & -(\omega_s - \omega) L_r J_2 & L_{sr} J_2 i_s \\ O_{1\times2} & L_{sr} i_s^T J_2 & 0 \end{pmatrix}$$

$$\mathcal{R}_D = \begin{pmatrix} R_s I_2 & O_{2\times2} & O_{2\times1} \\ O_{2\times2} & R_r I_2 & O_{2\times1} \\ O_{1\times2} & O_{1\times2} & B_r \end{pmatrix},$$

where L are inductances, R are resistances, lower indices s and r refer to stator and rotor respectively, B_r is the mechanical damping, i_s and $i_r \in \mathbb{R}^2$ are the stator and rotor currents and

$$J_2 = \begin{pmatrix} 0 & -1 \\ 1 & 0 \end{pmatrix} \in \mathbb{R}^{2\times2} \qquad I_2 = \begin{pmatrix} 1 & 0 \\ 0 & 1 \end{pmatrix} \in \mathbb{R}^{2\times2}. \tag{2}$$

Currents $i^T = (i_s^T, i_r^T) \in \mathbb{R}^4$ and fluxes Λ are related by $\Lambda = \mathcal{L} i$, where the inductance matrix $\mathcal{L}$ is

$$\mathcal{L} = \begin{pmatrix} L_s I_2 & L_{sr} I_2 \\ L_{sr} I_2 & L_r I_2 \end{pmatrix} \in \mathbb{R}^{4\times4}.$$

The interconnection matrix is

$$g_D = \begin{pmatrix} I_2 & O_{2\times2} \\ O_{2\times2} & I_2 \\ O_{1\times2} & O_{1\times2} \end{pmatrix} \in \mathbb{R}^{5\times4}$$

with the port variables $u^T = (v_s^T, v_r^T) \in \mathbb{R}^4$, where v_s, $v_r \in \mathbb{R}^2$ are the stator and rotor voltages. Finally, the Hamiltonian function is

$$H_D = \frac{1}{2} \Lambda^T \mathcal{L}^{-1} \Lambda + \frac{1}{2J_m} x_m^2.$$

2.2 The back-to-back converter

Fig. 2 shows the back-to-back converter selected for this system. It is made of a full bridge AC/DC single-phase boost-like rectifier and a 3-phase DC/AC inverter. The whole converter has an AC single-phase voltage input and its output are 3-phase PWM voltages which feed the rotor windings of the electrical machine. This system can be split into two parts: a dynamical subsystem (the full bridge rectifier, containing the storage elements), and an static subsystem (the inverter, which, from the energy point of view, acts like a transformer).

$v_i(t) = E \sin(\omega_s t)$ is a single-phase AC voltage source, L is the inductance (including the effect of any transformer in the source), C is the capacitor of the DC part, r takes into account all the resistance losses (inductor, source and switches), s_k and t_k, $k = 1, 2, 4, 5, 6$. Switch states take values in $\{-1, 1\}$ and t-switches are complementary to s-switches: $t_k = \bar{s_k} = -s_k$. Additionally, $s_2 = \bar{s_1} = -s_1$.

The PCHS averaged model of the full-bridge rectifier is as follows. The Hamiltonian variables are (B subindex refers to the B2B subsystem) $x_B^T = (\lambda_L, q) \in \mathbb{R}^2$, where λ_L is the inductor flux and q is the DC charge in the capacitor. The Hamiltonian function is

$$H_B = \frac{1}{2L} \lambda^2 + \frac{1}{2C} q^2,$$

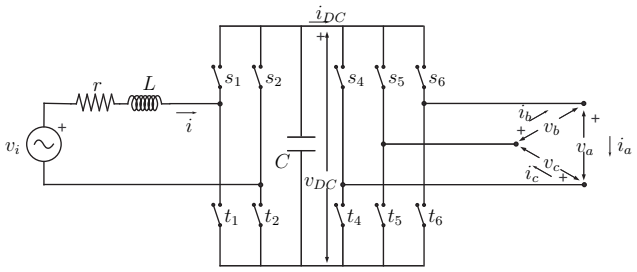

Figure 2: Back-to-back converter.

while the structure and damping matrices are

$$\mathcal{J}_B = \begin{pmatrix} 0 & -s_1 \\ s_1 & 0 \end{pmatrix} \in \mathbb{R}^{2\times 2} \quad \mathcal{R}_B = \begin{pmatrix} r & 0 \\ 0 & 0 \end{pmatrix} \in \mathbb{R}^{2\times 2}.$$

The interconnection matrix is

$$g_B = \begin{pmatrix} 1 & O_{1\times 3} \\ 0 & f^T \end{pmatrix} \in \mathbb{R}^{2\times 4}, \quad f = \frac{1}{2}\begin{pmatrix} s_6 - s_4 \\ s_5 - s_6 \\ s_4 - s_5 \end{pmatrix} \in \mathbb{R}^3,$$

with inputs

$$u = \begin{pmatrix} v_i \\ -i_{abc} \end{pmatrix} \in \mathbb{R}^4,$$

where $i_{abc}^T = (i_a, i_b, i_c) \in \mathbb{R}^3$ are the three-phase currents in the inverter part. Notice that the inverter subsystem can be seen as a Dirac structure [6] with

$$\begin{aligned} v_{abc} &= f v_{DC} \\ i_{DC} &= f^T i_{abc} \end{aligned}$$

where $v_{abc}^T = (i_a, i_b, i_c) \in \mathbb{R}^3$ are the three-phase voltages and $v_{DC} \in \mathbb{R}$, is the DC voltage, and $i_{DC} \in \mathbb{R}$ is the DC current supplied by the rectifier subsystem.

2.3 PCHS model of the whole system

The dq-transformation connects the B2B converter with the DFIM as a Dirac structure.

The interconnection relations are

$$\begin{aligned} v_r &= v_{dq} \\ i_r &= i_{dq} \\ v_{ABC} &= v_{abc} \\ i_{ABC} &= i_{abc}. \end{aligned} \tag{3}$$

We use equations (3) and introduce a new $\mathcal{K}$ matrix

$$\mathcal{K} = T_*^T e^{J_2(\delta-\theta)} \in \mathbb{R}^{3\times 2},$$

with T_* defined so as to remove the homopolar component,

$$T_* = \begin{pmatrix} \frac{\sqrt{2}}{\sqrt{3}} & -\frac{1}{\sqrt{6}} & -\frac{1}{\sqrt{6}} \\ 0 & \frac{1}{\sqrt{2}} & -\frac{1}{\sqrt{2}} \end{pmatrix} \in \mathbb{R}^{2\times 3},$$

and

$$e^{J_2\phi} = \begin{pmatrix} \cos(\phi) & -\sin(\phi) \\ \sin(\phi) & \cos(\phi) \end{pmatrix} \in \mathbb{R}^{2\times 2}.$$

The variables of the whole PCHS system are $x^T = (\Lambda^T, J_m\omega, \lambda, q) \in \mathbb{R}^7$, with energy function

$$H = H_D + H_B = \frac{1}{2}\Lambda^T\mathcal{L}^{-1}\Lambda + \frac{1}{2J_m}x_m^2 + \frac{1}{2L}\lambda^2 + \frac{1}{2C}q^2.$$

The $\mathbb{R}^{7\times 7}$ structure and dissipation matrices are

$$\mathcal{J} - \mathcal{R} = \begin{pmatrix} & & & O_{2\times 1} & O_{2\times 1} \\ & \mathcal{J}_D - \mathcal{R}_D & & O_{2\times 1} & \mathcal{K}^T f \\ & & & 0 & 0 \\ O_{1\times 2} & O_{1\times 2} & 0 & & \\ O_{1\times 2} & -f^T\mathcal{K} & 0 & \mathcal{J}_B - \mathcal{R}_B & \end{pmatrix},$$

and the interconnection matrix and port variables are

$$g = \begin{pmatrix} I_2 & O_{2\times 1} \\ O_2 & O_{2\times 1} \\ O_{1\times 2} & 0 \\ O_{1\times 2} & 1 \\ O_{1\times 2} & 0 \end{pmatrix} \in \mathbb{R}^{7\times 3} \qquad u^T = (v_s^T, v_i) \in \mathbb{R}^3.$$

3 Switching strategy

The power management schedule is determined according to the considerations presented in Section 1. The general goal is to supply the required power to the load with a high network power factor, *i.e.*, $Q_n \sim 0$. On the other hand, we will show below that the DFIM has an optimal mechanical speed for which there is minimal power injection through the rotor. Combining these two factors suggests to consider the following three modes of operation:

- **Generator mode.** When the real power required by the local load is bigger than the maximum network power (say, P_n^M) we use the DFIM as a generator. In this case we fix the references for the network real and reactive powers as $P_n^* = P_n^M$ and $Q_n^* = 0$.
- **Storage (or motor) mode.** When the local load does not need all the network power and the mechanical speed is far from the optimal value the "unused" power network is employed to accelerate the flywheel. From the control point of view, this operation mode coincides with the *generator mode*, and thus we fix the same references—but now we want to extract the maximum power from the network to transfer it to the flywheel.

- **Stand-by mode.** Finally, when the local load does not need all the power network and the mechanical speed is near to the optimal one we just compensate for the flywheel friction losses by regulating the speed and the reactive power. Hence, we fix the reference for the mechanical speed at its minimum rotor losses value (to be defined below) and set $Q_n^* = 0$.

The operation modes boil down to two kinds of control actions as expressed in Table 1, where P_l is the load power and $\epsilon > 0$ is some small parameter.

$P_n^* < P_l$	$\lvert\omega - \omega_s\rvert \leq \epsilon$	Mode	References
True	True	Generator	$P_n^* = P_n^M$ and $Q_n^* = 0$
True	False	Generator	$P_n^* = P_n^M$ and $Q_n^* = 0$
False	True	Stand-by	$Q_n^* = 0$ and $\omega^* = \omega_s$
False	False	Storage	$P_n^* = P_n^M$ and $Q_n^* = 0$

Table 1: Control action table.

To formulate mathematically the power flow strategy described above we need to express the various modes in terms of equilibrium points of the DFIM. In this way, the policy will be implemented transferring the system from one equilibrium point to another. Towards this end, we compute first the fixed points of the DFIM system (in subsection 2.1), *i.e.* the values Λ^* (or currents, $i = \mathcal{L}^{-1}\Lambda$), ω^*, v_r^* such that

$$\begin{pmatrix} -\omega_s L_s J_2 - R_s I_2 & -\omega_s L_{sr} J_2 & O_{2\times 1} \\ -\omega_s L_{sr} J_2 & -(\omega_s - \omega^*) L_r J_2 - R_r I_2 & L_{sr} J_2 i_s^* \\ O_{1\times 2} & L_{sr} i_s^{T*} J_2 & -B_r \end{pmatrix} \begin{pmatrix} i^* \\ \omega^* \end{pmatrix} + \begin{pmatrix} v_s \\ v_r^* \\ O_{1\times 2} \end{pmatrix} = 0.$$

Explicit separation of the rows corresponding to the stator, rotor, network and mechanical equations yields the following system of equations:

$$\omega_s L_s J_2 i_s^* + \omega_s L_{sr} J_2 i_r^* + R_s I_2 i_s^* - v_s = 0 \quad (4)$$

$$(\omega_s - \omega^*)(L_{sr} J_2 i_s^* + L_r J_2 i_r^*) + R_r I_2 i_r^* - v_r^* = 0 \quad (5)$$

$$L_{sr} i_s^{*\top} J_2 i_r^* - B_r \omega^* = 0. \quad (6)$$

It is clear that—assuming no constraint on v_r—the key equations to be solved are (4) and (6).

As discussed above, a DFIM has an optimal mechanical speed for which there is minimal power injection through the rotor. Indeed, from (5) one immediately gets

$$P_r^* \triangleq i_r^{*\top} v_r^* = (\omega_s - \omega^*) L_{sr} i_r^{*\top} J_2 i_s^* + R_r |i_r^*|^2,$$

where $|\cdot|$ is the Euclidean norm. Further, using (6), we get

$$P_r^* = B_r \omega^* (\omega^* - \omega_s) + R_r |i_r^*|^2. \quad (7)$$

Although the ohmic term in (7) does depend also on ω, its contribution is small for the usual range of parameter values, so $|P_r|$ is small near $\omega^* = \omega_s$. Another consideration that we make to justify our choice of "optimal" rotor speed, ω^*, concerns the reactive power supplied to the rotor—that we would like to minimize. It can be shown that

$$Q_r^* \triangleq i_r^{*\top} J_2 v_r^* = (\omega^* - \omega_s) f(Q_n, \omega^*),$$

where $f(\cdot,\cdot)$ is a bounded function of its arguments. Consequently, $Q_r^* = 0$ for $\omega^* = \omega_s$. Taking this into account, we will set the reference of the mechanical speed as $\omega^* = \omega_s$.

Let us explain now the calculations needed to determine the desired equilibria for the generating and stand–by modes. Assuming a sinusoidal steady–state regime, the network active and reactive powers are defined as

$$P_n \triangleq i_n^\top v_s = V_0 i_{nd} \tag{8}$$

$$Q_n \triangleq i_n^\top J_2 v_s = V_0 i_{nq}, \tag{9}$$

where $i_n = [i_{nd}, i_{nq}]^\top$.

In generator (and storage) mode we fix $P_n^* = P_n^M$ and $Q_n^* = 0$, and thus immediately obtain from (8) and (9) that $i_n^* = [\frac{P_n^M}{V_0}, 0]^\top$. Next, from network equations

$$i_l = i_n - i_s, \quad v_n = v_s \tag{10}$$

and the measured i_l we obtain i_s^* which, upon replacement on (4) yields i_r^*. Then, ω^* is computed from (6), and finally v_r^* is obtained via (5).

For the stand–by mode we still set $Q_n^* = 0$, but now fix $\omega^* = \omega_s$. This is a more complicated scenario as we have to ensure the existence of i_s^* and i_r^* solutions for the nonlinear equations (4) and (6). First of all, multiplying equation (4) by $i_s^{*\top}$ and using equation (6) one gets

$$R_s |i_s^*|^2 - v_s^\top i_s^* + B_r \omega_s^2 = 0. \tag{11}$$

This is a quadratic equation in the two components of i_s^*. It may have an infinite number of solutions, a unique one, or no solution at all, depending on whether ω_s is smaller, equal or larger than $\frac{V_0}{\sqrt{2}B_r R_s}$, respectively. Since B_r is usually a small coefficient typically there will be an infinite number of i_s^* that solve the equation. We will choose then the one of minimum norm. Once we have fixed i_s^* we can proceed as in the generating mode to compute i_r^* and v_r^*.

Before closing this section we make the observation that, under the assumptions that the load can be modelled as a linear RL circuit and small friction coefficient, we can get a simple condition on the load parameters that ensure the existence of ω^* and P_n^*, with $Q_n^* = 0$. Indeed, taking a general RL-load

$$Z_l = R_l I_2 + \omega_s L_l J_2,$$

replacing in (11), using (10), and the network power definitions (8), (9) we obtain

$$(P_n^*)^2 - |v_s|^2 \left(\frac{2R_l}{|Z_l|^2} + \frac{1}{R_s} \right) P_n^* + \frac{|v_s|^4}{|z_l|^2} \left(1 + \frac{R_l}{R_s} + \frac{2\omega_s L_l Q_n^*}{|v_s|^2} \right) - \frac{|v_s|^2 B_r \omega_s^2}{R_s} = 0.$$

In our case $Q_n^* = 0$ and considering $B_r = 0$ yields the quadratic equation

$$(P_n^*)^2 - |v_s|^2 \left(\frac{2R_l}{|Z_l|^2} + \frac{1}{R_s} \right) P_n^* + \frac{|v_s|^4}{|Z_l|^2} \left(1 + \frac{R_l}{R_s} \right) = 0.$$

It is easy to show that this equation has a positive real solution if and only if

$$R_s < \frac{R_l^2}{2\omega_s L_l} + \frac{\omega_s L_l}{2}, \tag{12}$$

and hence it always has a real solution for loads with sufficiently small inductance.

DFIM	L_{sr}	L_r, L_s	J_m	B_r	R_s	R_r	v_g
Value	0.041	0.042	5.001	0.005	0.087	0.0228	$(380, 0)$

B2B	r	L	C	E
Value	0.08	$1 \cdot 10^{-3}$	$4.5 \cdot 10^{-3}$	68.16

Table 2: Simulation parameter values (in SI units) for the DFIM and the B2B. Additionally, $\omega_s = \omega_o = 2\pi 50$.

4 Simulations

In this Section we implement a numerical simulation of the whole system controlled via the IDA-PBC. These control laws are presented in previous deliverables, and also can be found in [5] and [3]. The simulation has been performed using the *20-sim*[1] modelling and simulation software. The parameters used in the simulations are given in Table 2.

A resistive-inductive varying load is simulated. The load is initially $R_l = 1000$, $L_l = 0.01$, changes to $R_l = 1$ at $t = 1$ in 0.2 seconds, and returns to $R_l = 1000$ at $t = 1.8$, also in 0.2 seconds.

For the purposes of testing the controller, a maximum power network of $P_n^M = 10000$ and a desired bus voltage $v_{DC}^* = 150$ have been set. The damping parameter is fixed at $r = 25$.

Fig. 3 shows the power required from the load P_l and the active power supplied by the network P_n. Even if P_l is bigger than the maximal power (P_n^M), P_n does not overcome P_n^M. The mechanical speed during the load changes is depicted in Fig. 3. Notice that in the stand-by mode ω is kept at $\omega_s = 2\pi 50 \frac{rad}{s}$. Fig. 4 shows the reactive power compensation of the whole system.

Fig. 5 shows v_{DC}, which indeed remains close to v_{DC}^*. Finally, voltage v_i and current i at the single phase source feeding the B2B are depicted in Fig. 6, showing that they are nearly in phase.

5 Conclusions

We have established the stability of the equilibrium points corresponding to the three operating modes described in Table 1. The system not only provides the active power required by the load, but at the same time compensates the reactive power, so that the power grid sees the load+machine system as a pure resistive load, even for varying inductive local loads. There is no actual restriction about the kind of local load, as long as its parameters allow the assignment of equilibrium points.

However, stability cannot be ensured, without further analysis, when the power flow strategy that switches the operating modes is in place. If the switching is replaced by a smooth, sufficiently slow, transition from one operating point to the other we can invoke total stability arguments to prove that stability is preserved under some additional uniformity assumptions. Completing this analysis is the subject of on–going research.

[1] See `www.20sim.com`

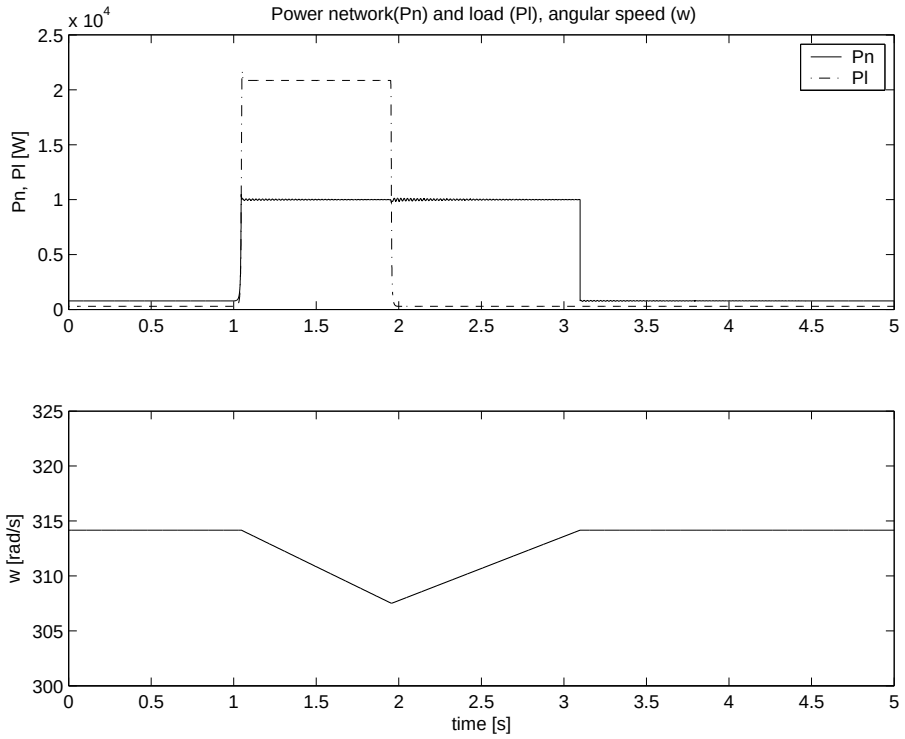

Figure 3: Upper: power network P_n and power load P_l. Lower: mechanical speed ω.

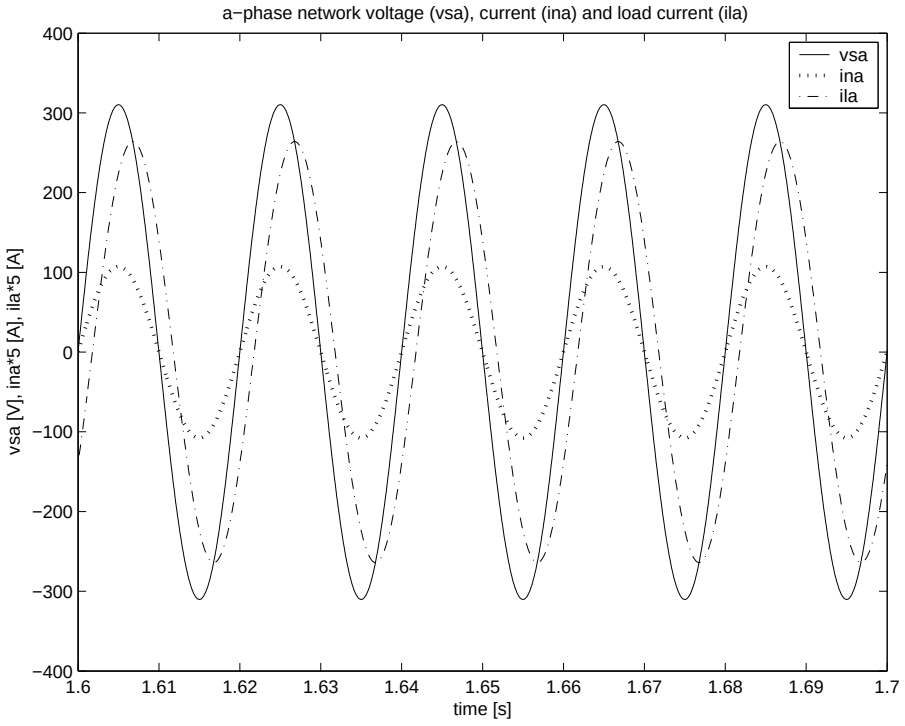

Figure 4: Detail of the grid a-phase voltage v_{sa} and current i_{na}, and load current i_{la}.

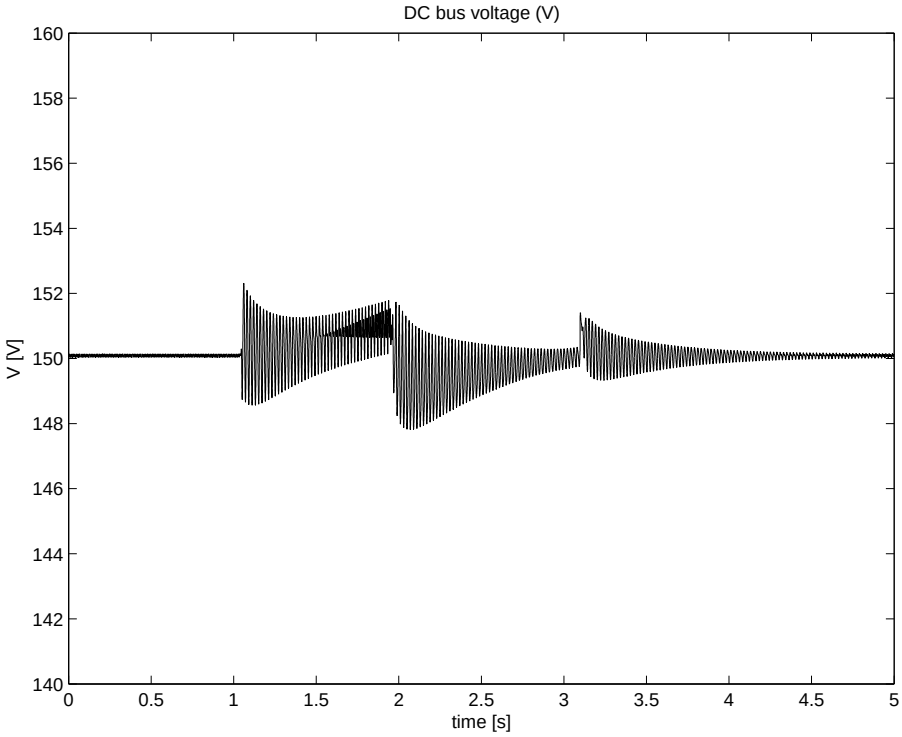

Figure 5: DC-bus voltage v_{DC} of the B2B.

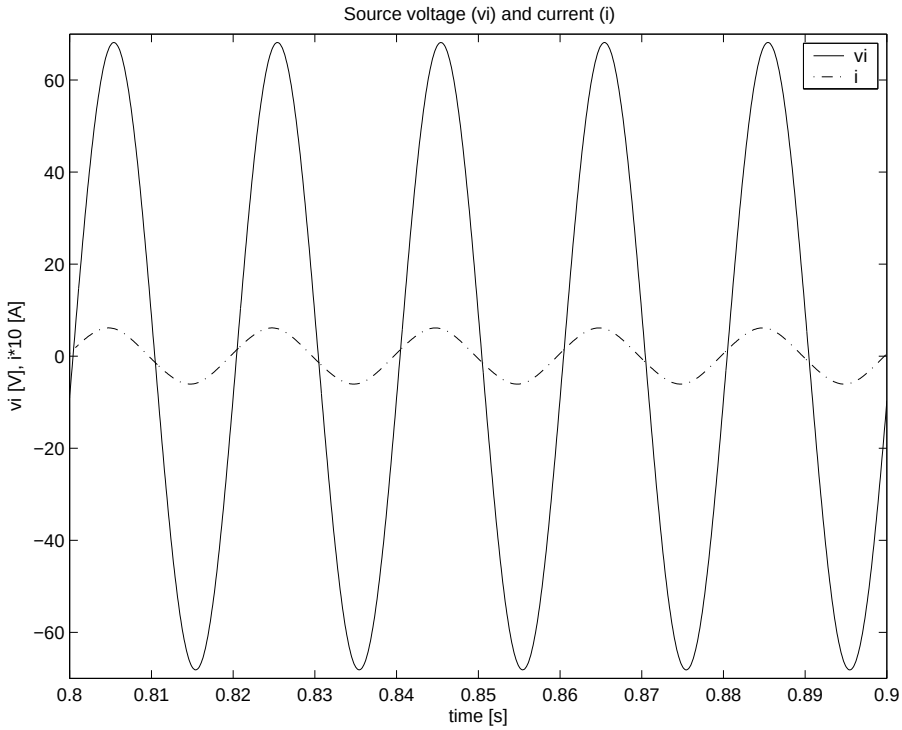

Figure 6: Detail of the AC single-phase voltage and current for the B2B.

References

[1] H. Akagi and H. Sato. Control and performance of a doubly-fed induction machine intended for a flywheel energy storage system. *IEEE Trans. Power Electron.*, 17(1):109–116, 2002.

[2] C. Batlle and A. Dòria-Cerezo. Energy-based modelling and simulation of the interconnection of a back-to-back converter and a doubly-fed induction machine. In *Accepted to the 2006 American Control Conference*, 2006.

[3] C. Batlle, A. Dòria-Cerezo, and E. Fossas. IDA-PBC controller for a bidirectional power flow full-bridge rectifier. In *IEEE Proc. Conference on Decision and Control*, 2005.

[4] C. Batlle, A. Dòria-Cerezo, and R. Ortega. Power Flow Control of a Doubly–Fed Induction Machine Coupled to a Flywheel. In *IEEE Proc. Conference on Control Applications*, pages 1645–1651, 2004.

[5] C. Batlle, A. Dòria-Cerezo, and R. Ortega. Power Flow Control of a Doubly–Fed Induction Machine Coupled to a Flywheel. *European Journal of Control*, 11(3):209–221, 2005.

[6] M. Dalsmo and A. van der Schaft. On representations and integrability of mathematical structures in energy-conserving physical systems. *SIAM J. Control Optim.*, 37:54–91, 1998.

[7] B. Hopfensperger, D. Atkinson, and R. Lakin. Stator-flux-oriented control of a doubly-fed induction machine with and without position encoder. In *IEE Proc. Electric Power Applications*, volume 147-4, pages 241–250, 2000.

[8] P. C. Krause. *Analysis of electric machinery*. McGraw-Hill, 1986.

[9] R. Peña, J. C. Clare, and G. M. Asher. Doubly fed induction generator using back-to-back pwm converters and its application to variable speed wind-energy generation. In *IEEE Proc. Electric Power Applications*, volume 143-5, pages 231–241, 1996.

[10] R. Peña, J. C. Clare, and G. M. Asher. A doubly fed induction generator using back-to-back pwm converters supplying an isolated load from a variable speed wind turbine. In *IEEE Proc. Electric Power Applications*, volume 143-5, pages 380–387, 1996.

[11] S. Peresada, A. Tilli, and A. Tonelli. Indirect Stator Flux-Oriented Output Feedback Control of a Doubly Fed Induction Machine. *IEEE Trans. Control Systems Technology*, 11(6):875–888, 2003.

[12] S. Peresada, A. Tilli, and A. Tonelli. Power control of a doubly fed induction machine via output feedback. *Control Engineering Practice*, 12:41–57, 2004.

[13] A. Tapia, G. Tapia, J. X. Ostolaza, and J. R. Sáenz. Modeling and control of a wind turbine driven doubly fed induction generator. *IEEE Trans. Energy Conversion*, 18:194–204, 2003.

[14] A. van der Schaft. *L_2 gain and passivity techniques in nonlinear control*. Springer, 2000.

[15] L. Xu and W. Cheng. Torque and reactive power control of a doubly fed induction machine by position sensorless scheme. *IEEE Trans. Industry Applications*, 31(3):636–642, 1995.